JACC: BASIC TO TRANSLATIONAL SCIENCE VOL. 9, NO. 5, 2024

LEADING EDGE TRANSLATIONAL RESEARCH

miR-590-3p Overexpression Improves the Efficacy of hiPSC-CMs for Myocardial Repair

Zhiwei Zhang, MD,[a,*] Xiaoting Li, MD,[b,c,*] Jiawei Zhuang, MD,[d] Qingwei Ding, MD,[a] Hui Zheng, MD,[a] Teng Ma, MD,[a] Qingyou Meng, MD,[a] Ling Gao, PhD[e]

VISUAL ABSTRACT

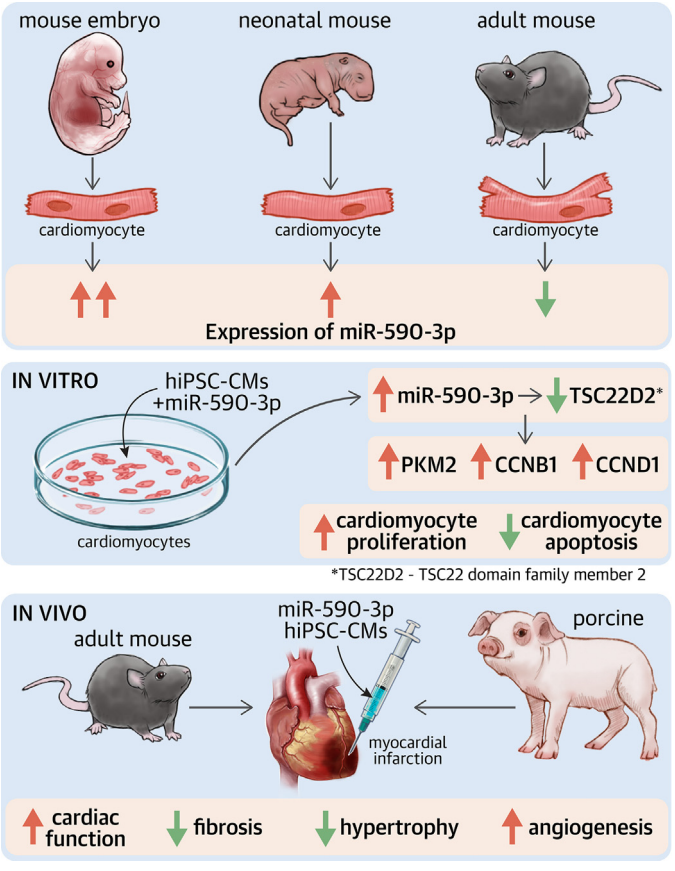

Zhang Z, et al. J Am Coll Cardiol Basic Trans Science. 2024;9(5):557-573.

HIGHLIGHTS

- **miR-590-3p overexpression increased the proliferative capacity of hiPSC-CMs in vitro and in vivo.**
- **miR-590-3p overexpression enhanced the number of engrafted hiPSC-CMs in infarcted mouse hearts.**
- **miR-590-3p-overexpressing hiPSC-CMs promoted cardiac repair in a preclinical pig MI model.**

From the [a]Department of Vascular Surgery, General Surgery Clinical Center, Shanghai General Hospital, Shanghai Jiao Tong University School of Medicine, Shanghai, China; [b]Department of Geriatrics, Shanghai General Hospital, Shanghai Jiao Tong University School of Medicine, Shanghai, China; [c]Department of Cardiology, Second Affiliated Hospital of Soochow University, Suzhou, China; [d]Department of Cardiovascular Surgery, The First Affiliated Hospital of Xiamen University, School of Medicine,

ISSN 2452-302X https://doi.org/10.1016/j.jacbts.2023.11.005

ABBREVIATIONS AND ACRONYMS

BLI = bioluminescence live imaging

ECM = extracellular matrix

HF = heart failure

hiPSC-CM = human induced pluripotent stem cell-derived cardiomyocyte

LAD = left anterior descending coronary artery

LVEDV = left ventricular end-diastolic volume

LVESV = left ventricular end-systolic volume

MI = myocardial infarction

miRNA = microRNA

OE = overexpressing

qRT-PCR = quantitative real-time polymerase chain reaction

UTR = untranslated region

SUMMARY

Recent evidence demonstrates that low engraftment rates limit the efficacy of human induced pluripotent stem cell–derived cardiomyocytes (hiPSC-CMs) for cardiac repair after myocardial infarction. In this study, we attempted to overcome this limitation by enhancing the proliferative capacity of transplanted hiPSC-CMs. We found that miR-590-3p overexpression increased the proliferative capacity of hiPSC-CMs. miR-590-3p overexpression increased the number of engrafted cells and had a higher efficacy for myocardial repair than control cells. Moreover, we confirmed the safety of using miR-590-3p-overexpressing hiPSC-CMs in pig hearts. These results indicated that miR-590-3p overexpression stimulated hiPSC-CM cell cycle re-entry to induce cell proliferation and increased the therapeutic efficacy in MI. (J Am Coll Cardiol Basic Trans Science 2024;9:557–573)

Despite significant advances in disease management, end-stage heart failure (HF) is the leading cause of mortality worldwide because of the limited regenerative capacity of the adult human heart.[1] In mammals, the proliferative capacity of cardiomyocytes ceases in a short window after birth.[2] As a result, injured hearts have a limited ability to repair because they produce a limited number of cardiomyocytes after myocardial infarction (MI). Consequently, the ischemic site is replaced by scar tissue without contractile function. In recent years, concerted efforts have been made to develop therapeutic strategies to promote myocardial regeneration. Several advanced approaches, including adult/somatic stem cell transplantation, induction of the proliferation of endogenous cardiomyocytes, and the transdifferentiation of resident cardiac fibroblasts into functional cardiomyocyte-like cells, can improve cardiac function and reduce cardiac fibrosis in animal models of MI.[3-5] However, the therapeutic efficacy of these methods is limited, and these strategies have safety concerns, such as an increased risk of ventricular arrhythmia.[6] Therefore, it is crucial to develop novel, efficient, and safe therapeutic strategies to promote cardiac regeneration.

Transplanting human induced pluripotent stem cell-derived cardiomyocytes (hiPSC-CMs) into injured myocardium is promising for end-stage HF treatment. Unlike adult human cardiomyocytes, hiPSCs have unlimited self-renewal capacity and can readily differentiate into cardiomyocytes in vitro under certain induction conditions. Theoretically, producing a clinically relevant number of hiPSC-CMs is feasible through industrialization. CMs derived from hiPSCs are structurally and functionally immature, resembling fetal CMs, with a gene expression profile of a developing heart, small cell size, less organized sarcomeres, small forces of contraction, and low mitochondrial density compared with adult CMs.[7] In addition, although the long-term culture of hiPSC-CMs stimulates cell maturation to some extent,[8] metabolic maturation reduces the proliferation of hiPSC-CMs and their ability to tolerate hypoxia.[7] As a result, only a small percentage of transplanted cells survive at the injection sites, preventing harnessing the full potential of hiPSC-CMs in cardiac regeneration.[9] Therefore, developing novel approaches to enhance the engraftment rate of hiPSC-CMs during cardiovascular disease treatment is critical.

MicroRNAs (miRNAs) are evolutionarily conserved, single-stranded, noncoding, 18- to 22-nucleotide RNAs that regulate gene expression by directly binding to the 3′-untranslated regions (UTRs) of target messenger RNAs.[10] miRNAs participate in various biological processes, including embryonic development and tissue regeneration.[11,12] Additionally, miRNAs have essential functions in heart regeneration. For instance, miR-19a/19b promoted endogenous cardiomyocyte proliferation by regulating the expression of phosphatase and tensin

Xiamen University, Xiamen, China; and the [e]Translational Medical Center for Stem Cell Therapy and Institute for Regenerative Medicine, Shanghai East Hospital, Tongji University School of Medicine, Shanghai, China. *Drs Zhang and Li contributed equally to this work.

The authors attest they are in compliance with human studies committees and animal welfare regulations of the authors' institutions and Food and Drug Administration guidelines, including patient consent where appropriate. For more information, visit the Author Center.

Manuscript received July 13, 2023; accepted November 22, 2023.

homolog deleted on chromosome 10 (PTEN) in a mouse model of MI.[13] However, AAV6-miR-199a administration led to uncontrolled cardiac regeneration in a pig model of MI.[6]

The role of miRNAs in regulating hiPSC-CM physiology remains largely unknown. A previous study performed miRNA functional screening and found that miR-590-3p promoted cardiomyocyte proliferation.[12] In addition, Lesizza et al[14] reported that AAV6-miR-590-3p stimulated endogenous cardiomyocyte proliferation and improved cardiac function after MI. However, little is known about the effect of miR-590-3p on hiPSC-CM proliferation. In this study, we investigated: 1) the ability of miR-590-3p to stimulate hiPSC-CM proliferation; 2) the potential to transplant miR-590-3p-overexpressing (OE) hiPSC-CMs into mouse and pig hearts; and 3) the ability of miR-590-3p-OE hiPSC-CMs to promote cardiac repair in mouse and pig models of MI.

METHODS

hiPSC CULTURE AND CARDIOMYOCYTE DIFFERENTIATION. The hiPSC line RC01001-A (Nuwacell) was used in this study. hiPSCs were maintained in Essential 8 medium (Stemcell Technologies) and differentiated into cardiomyocytes using the GiWi protocol.[15] Differentiated hiPSC-CMs were purified by metabolic selection between day 15 and day 25, as described previously.[15] The purity of hiPSC-CMs was confirmed by flow cytometry using a FACSCalibur flow cytometer (Beckman Coulter). The maturation of differentiated hiPSC-CMs was achieved by prolonging the culture period (up to day 60).

PRODUCTION AND TRANSFECTION OF AAV6-miR-590-3P. The plasmids AAV6-miR-590-3p and control AAV6 were purchased from GeneChem Technologies. AAV packaging was conducted using AAV-293 cells, and AAV particles were harvested from the supernatant using an AAV Purification Maxi Slurry Kit (AmyJet Scientific). The concentration of particles was adjusted (1:100 to 1:1,000 dilution) to minimize cell toxicity and achieve transfection efficiencies of >80%. After transfection, the expression of miR-590-3p in hiPSC-CMs was detected by quantitative real-time polymerase chain reaction (qRT-PCR).

FLUORESCENCE IN SITU HYBRIDIZATION. Fluorescence in situ hybridization assays were performed to detect miR-590-3p in heart tissues according to the manufacturer's instructions. Briefly, heart samples were embedded in an optimal cutting temperature compound for serial cryosectioning. The sections (8 μm thick) were incubated with proteinase K (15 μg/mL) at 37 °C for 30 minutes. Then, miR-590-3p was hybridized with a Cy3-labeled oligonucleotide probe (AmyJet Scientific). The sections were stained with 4',6-diamidino-2-phenylindole and imaged under an inverted fluorescence microscope (Leica).

IMMUNOFLUORESCENCE ANALYSES. Cell or tissue samples were fixed with 4% paraformaldehyde and permeabilized with 0.4% Triton X-100 at room temperature for 15 minutes. After nonspecific antigen blocking with 1% bovine serum albumin for 1 hour, the samples were incubated with primary antibodies (for details, see Supplemental Table 1) at 4 °C overnight and subsequently incubated with the corresponding secondary antibodies at 37 °C for 2 hours. Wheat germ agglutinin (Thermo Fisher Scientific) and terminal deoxynucleotidyl transferase-mediated deoxyuridinetriphate nick-end labeling (Thermo Fisher Scientific) staining were performed using a commercial kit. Nuclei were stained with 4',6-diamidino-2-phenylindole.

MESSENGER RNA PROFILING. RNA sequencing of control and miR-590-3p-OE hiPSC-CMs was performed using an Illumina 2000 and 2 × 100-base pair paired-end sequencing (LC Sciences) as described previously. Gene ontology enrichment analysis of differentially expressed genes was performed using the Lianchuan Biological Cloud Platform (LC Sciences).

ANIMAL EXPERIMENTS. Mice MI was induced in a mouse model by ligating the left anterior descending coronary artery (LAD) as described previously. Briefly, M-NSG (NOD-Prkdc^{scid}Il2rg^{em1}/Smoc) female mice (9-10 weeks old, provided by Shanghai Model Organisms Center) were anesthetized with 2% isoflurane and mechanically ventilated using an animal ventilator (Harvard Apparatus). The heart was exposed by left thoracotomy, and the LAD was ligated using an 8-0 Prolene suture (Ethicon). The animals were randomly divided into 3 groups: an MI group (15 μL of phosphate-buffered saline), a control group (5.0 × 10^5 wild-type hiPSC-CMs), and an miR-590-3p group (5.0 × 10^5 miR-590-3p-OE hiPSC-CMs). After cell delivery, the incisions were closed with 6-0 sutures. A sham group underwent all procedures except LAD ligation.

Bama pigs (female; 20-25 kg) were used to evaluate the therapeutic effect of hiPSC-CM transplantation on MI. Briefly, pigs were anesthetized with 2% isoflurane and mechanically ventilated using an animal ventilator (Hallowell EMC). The heart was exposed by left thoracotomy, and the LAD was occluded between the first and second diagonal coronary arteries with a 4-0 Prolene suture for 1 hour and then reperfused. miR-590-3p-OE hiPSC-CMs or control cells (5.0 × 10^7

cells/heart, 8-10 points in the injured area) were injected into the myocardium, and the incision was closed. The animals received the following immunosuppressants: methylprednisolone sodium succinate (2 mg/kg), tacrolimus (0.3 mg/kg), and mycophenolate mofetil (100 mg/kg). A telemetry device (Ensense Biomedical Technologies) was implanted subcutaneously in the chest wall according to the manufacturer's instructions. The peripheral blood of each pig was collected and analyzed at the Department of Clinical Pathology of Shanghai General Hospital.

CARDIAC FUNCTION ANALYSES. Mice. Cardiac function was assessed by echocardiography at indicated timepoints. Mice were anesthetized with 2% isoflurane and mechanically ventilated. Echocardiography data were measured using a Visual Sonics Vevo2100 system (Visual Sonics). Left ventricular ejection fraction and fractional shortening were calculated using the following equations: ejection fraction percentage = [(LVEDV − LVESV)/LVEDV] × 100 and fractional shortening percentage = [(LVEDD − LVESD)/LVEDD] × 100, where LVEDV and LVESV are left ventricular end-diastolic and end-systolic volume, respectively, and LVEDD and LVESD are left ventricular end-diastolic and end-systolic diameter, respectively. An operator blinded to the study groups performed all measurements.

Pigs. Cardiac function was assessed by high-resolution computed tomography (Siemens). Briefly, the animals were anesthetized with 2% isoflurane and placed in the supine position. Before computed tomography scanning, an iodinated contrast agent (0.5 mL/kg; Abcam) was injected into the ear vein. Cardiac function was analyzed with Vitrea Enterprise Suite software (Siemens).

CELL ENGRAFTMENT. The engraftment of implanted hiPSC-CMs was evaluated by bioluminescence live imaging (BLI), immunofluorescent staining, and qRT-PCR. In BLI, luciferase-hiPSC-CMs were evaluated using the IVIS Lumina III In Vivo Imaging System (PerkinElmer) 7 and 28 days after cell delivery. The average fluorescence intensity of regions of interest was quantitated. For histologic analysis, hiPSC-CMs were stained with human-specific cardiac troponin T and imaged using an inverted fluorescence microscope. The expression of the sex-determining region Y (*SRY*) gene in the transplantation site was measured to evaluate the engraftment rate of implanted hiPSC-CMs, as described previously.

QUANTITATIVE REAL-TIME POLYMERASE CHAIN REACTION. Total RNA isolation, reverse transcription, and qRT-PCR were performed as described previously. Glyceraldehyde-3-phosphate dehydrogenase or U6 small nuclear RNA (for miRNA) served as internal controls. The primer sequences are listed in Supplemental Table 2.

WESTERN BLOT. Protein isolation, quantitation, and electrophoresis were performed as described previously. Glyceraldehyde-3-phosphate dehydrogenase served as a loading control. Protein blots were analyzed by Image Pro Plus version 6.0.

DUAL-LUCIFERASE REPORTER ASSAY. hiPSC-CMs (5.0×10^4 cells/well) were seeded in 24-well plates and cotransfected with TSC22D2 luciferase reporter plasmids and miR-590-3p mimic or negative control using Lipofectamine 3000 (Thermo Fisher Scientific). After 48 hours, luciferase activity was detected using a dual-luciferase reporter assay system (Promega). *Renilla* luciferase activity was used as an internal control.

STATISTICAL ANALYSIS. Data are presented as mean ± SD and analyzed using Graph Pad Prism software version 9.0 (GraphPad Software Inc). The Shapiro-Wilk test was used to assess normality. The unpaired Student's *t*-test was used for comparisons between 2 groups, and 1-way analysis of variance followed by the Tukey' post hoc test for multiple pairwise comparisons was used for comparisons among >2 groups unless otherwise specified. Pearson's correlation coefficient (*r* values with 95% CIs) was used to compare continuous variables. A P value of <0.05 was considered statistically significant.

STUDY APPROVAL. Human experiments were approved by the Research Ethics Committee of Shanghai Jiao Tong University. Fetal heart tissues were collected after elective surgical abortions. Adult heart tissues (controls) were obtained from patients who died without cardiac disease. The spouse or immediate family of heart donors provided written informed consent.

All animal experiments were approved by the Institutional Animal Care and Use Committee of Shanghai Jiao Tong University and were performed in accordance with the National Institutes of Health Guide for the Care and Use of Laboratory Animals.

RESULTS

miR-590-3P IS ENRICHED IN THE FETAL HEART. To assess the role of miR-590-3p in the cardiomyocyte cell cycle, we first measured its expression in human hearts. Our results showed that miR-590-3p expression was significantly higher in fetal hearts than in adult hearts. Not surprisingly, the expression of the

FIGURE 1 miR-590-3p Expression in Cardiomyocytes

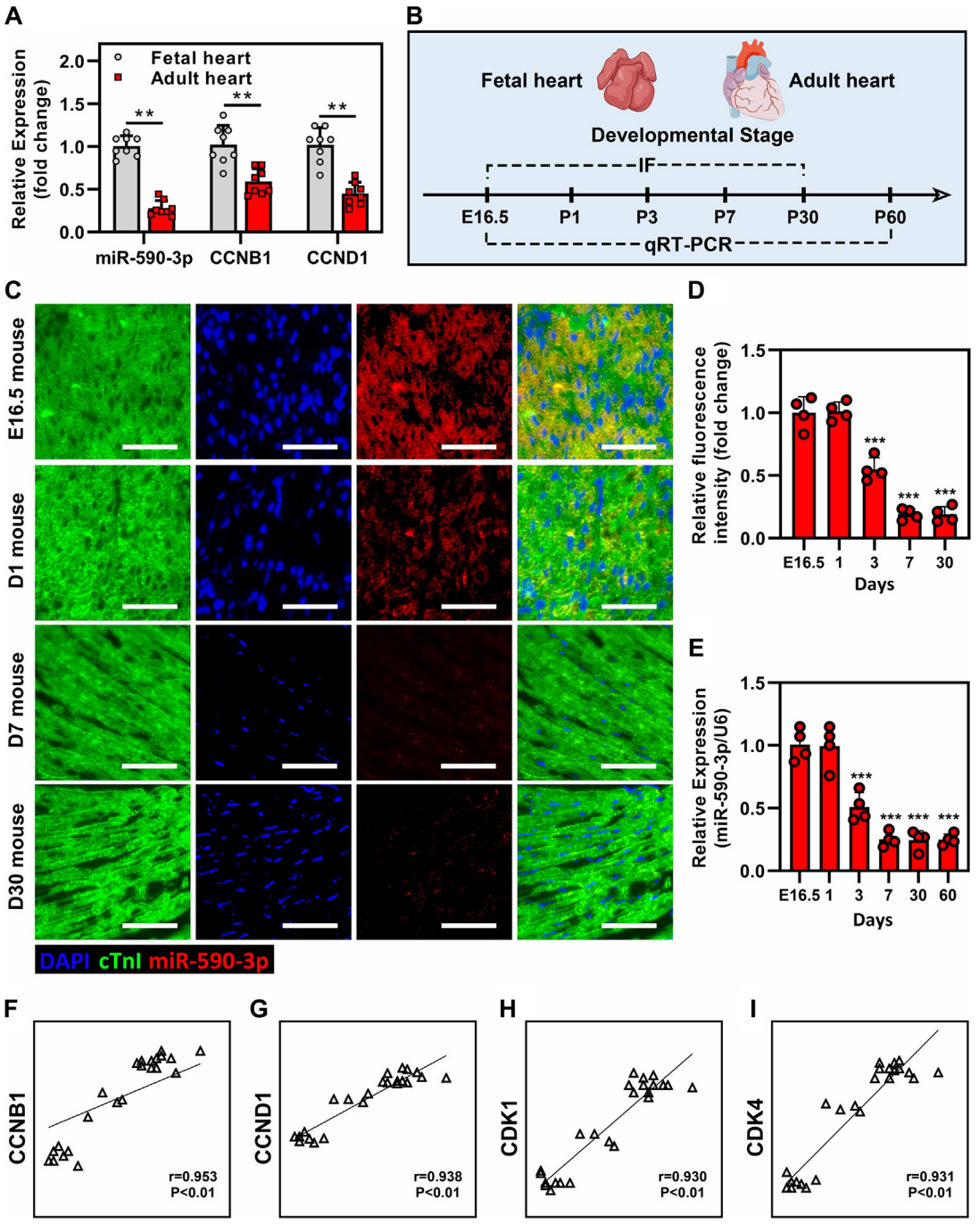

(A) Relative expression levels of miR-590-3p, *CCNB1*, and *CCND1* in human hearts detected by qRT-PCR (n = 8). (B) Stages of heart development. (C) The expression of miR-590-3p at different stages of mouse heart development was detected by fluorescence in situ hybridization. Scale bar = 100 μm. (D) Quantitative analysis of miR-590-3p fluorescence intensity (embryos at 16.5 days and day 1, day 3, day 7, or day 30 after birth; n = 4). (E) Relative expression of miR-590-3p in mouse hearts detected by qRT-PCR at indicated timepoints (embryos at 16.5 days and day 1, day 3, day 7, day 30, or day 60 after birth; n = 4). (F to I) Correlations between the expression levels of miR-590-3p, *CCNB1*, *CCND1*, *CDK1*, and *CDK4* in mouse hearts (n = 24). Data are presented as mean ± SD. *P* values were determined using the unpaired Student's *t*-test or 1-way repeated-measures analysis of variance followed by Dunnett's post hoc test. $^{**}P < 0.01$ and $^{***}P < 0.001$ vs E16.5. CCNB1 = cyclin B1; CCND1 = cyclin D1; CDK1 = cyclin-dependent kinase 1; CDK4 = cyclin-dependent kinase 4; D = day; E = embryonic day; FISH = fluorescence in situ hybridization; IF = immunofluorescence; miR = microRNA; P = postnatal day; qRT-PCR = quantitative real-time polymerase chain reaction.

proliferation genes cyclin B1 (*CCNB1*) and cyclin D1 (*CCND1*) was also significantly higher in fetal hearts than in adult hearts (Figure 1A). Next, we detected the expression of miR-590-3p during mouse cardiac development by fluorescence in situ hybridization and qRT-PCR (Figure 1B). The miRNA fluorescence in situ hybridization assay demonstrated that miR-590-3p was enriched in fetal mouse hearts (Figures 1C and 1D). Moreover, our qRT-PCR results demonstrated that miR-590-3p expression was up-regulated in mouse embryonic hearts and decreased after birth (Figure 1E). We also investigated the correlation between the expression of miR-590-3p and proliferation-related genes in mouse hearts at different developmental stages. The expression of *CCNB1*, *CCND1*, cyclin-dependent kinase (*CDK*) 1, and *CDK4* was linearly correlated with that of miR-590-3p (Figures 1F to 1I).

miR-590-3p OVEREXPRESSION PROMOTED hiPSC-CM PROLIFERATION. Next, we investigated whether miR-590-3p overexpression promoted the proliferation of hiPSC-CMs. For this purpose, hiPSCs were differentiated into cardiomyocytes using the GiWi protocol (Supplemental Figure 1A). miR-590-3p overexpression was induced by AAV6-miR-590-3p transfection and confirmed by qRT-PCR 10 days after transfection (Supplemental Figure 1B). We found that miR-590-3p-OE hiPSC-CMs were immature (Supplemental Figures 1C to 1E). Immunofluorescence analyses indicated that miR-590-3p overexpression significantly increased the proportion of cells expressing proliferation markers (Figures 2A to 2D).

We also assessed the effect of miR-590-3p on cell apoptosis. The results revealed that miR-590-3p overexpression reduced the number of apoptotic (transferase-mediated deoxyuridinetriphate nick-end labeling-positive) cells in an ischemic and hypoxic environment (Figures 2E and 2F). Moreover, qRT-PCR analysis showed that miR-590-3p overexpression up-regulated G1/S genes (*CCND1* and *CDK4*) and G2/M genes (*CCNA1* and polo-like kinase 1 [*PLK1*]) (Figures 2G and 2H), up-regulated the anti-apoptotic gene *Bcl-2*, and down-regulated the pro-apoptotic gene *Bax* in hiPSC-CMs (Figure 2I).

miR-590-3p overexpression up-regulated 1,304 genes and down-regulated 1,192 genes (Supplemental Figures 2A to 2C). These genes were implicated in cellular structure, excitation-contraction coupling, and metabolism. Gene ontology enrichment analysis showed that miR-590-3p overexpression affected various biological processes, including cell proliferation and apoptosis (Supplemental Figure 2D). These results are consistent with the ability of miR-590-3p to stimulate cellular proliferation and inhibit apoptosis.

miR-590-3P PROMOTED hiPSC-CM PROLIFERATION BY REGULATING THE TSC22D2/PKM2 PATHWAY. The molecular mechanism by which miR-590-3p regulates hiPSC-CM proliferation was investigated. We performed a bioinformatics analysis to identify target genes using 4 target gene prediction databases. Ankyrin repeat and SOCS box containing 1 (*ASB1*), transmembrane protein 18 (*TMEM18*), and TSC22 domain family member 2 (*TSC22D2*) were found in all databases (Figure 3A). The results of qRT-PCR showed that miR-590-3p decreased the expression of *TMEM18* and *TSC22D2* in hiPSC-CMs (Figure 3B). Further, TSC22D2 expression was higher in cardiomyocytes than in cardiac fibroblasts and endothelial cells (Figure 3C). Therefore, we selected *TSC22D2* for further studies and performed a dual-luciferase reporter assay to assess whether *TSC22D2* was a downstream target of miR-590-3p (Figure 3D). Our results showed that the relative luciferase activity decreased significantly in cells expressing TSC22D2 and miR-590-3p (Figure 3E). A recent study reported that TSC22D2 inhibited cellular proliferation by regulating pyruvate kinase M2 (PKM2).[16] Relative protein expression was measured by Western blot analysis. The findings demonstrated that miR-590-3p down-regulated TSC22D2 expression and up-regulated PKM2, cyclin B1, and cyclin D1, which regulate cell proliferation (Figure 3F). Immunofluorescence staining showed that TSC22D2 overexpression reversed the effect of miR-590-3p on hiPSC-CM proliferation (Figures 3G and 3H).

miR-590-3p–OE hiPSC-CMs IMPROVED CARDIAC FUNCTION IN A MURINE MODEL OF MI. To investigate whether miR-590-3p overexpression could enhance the therapeutic efficacy of hiPSC-CMs in myocardial repair, we evaluated the cardiac function of mice treated with miR-590-3p-OE hiPSC-CMs (miR-590-3p) or control hiPSC-CMs (control) (Figure 4A). Treatment with control hiPSC-CMs decreased the heart weight/body weight ratio, and miR-590-3p potentiated this effect (Figure 4B). Echocardiographic measurements indicated that control hiPSC-CMs improved cardiac function on day 28 post-MI, and miR-590-3p enhanced this effect (Figures 4C to 4G). The scar size was quantified by histology (Masson's tricolor staining). Control hiPSC-CMs decreased the fibrotic area, and miR-590-3p overexpression enhanced this effect (Figures 4H and 4I). These findings demonstrated that miR-590-3p overexpression increased the

FIGURE 2 **miR-590-3p Overexpression Promotes the Proliferation of hiPSC-CMs and Increases Their Ability to Tolerate Hypoxia In Vitro**

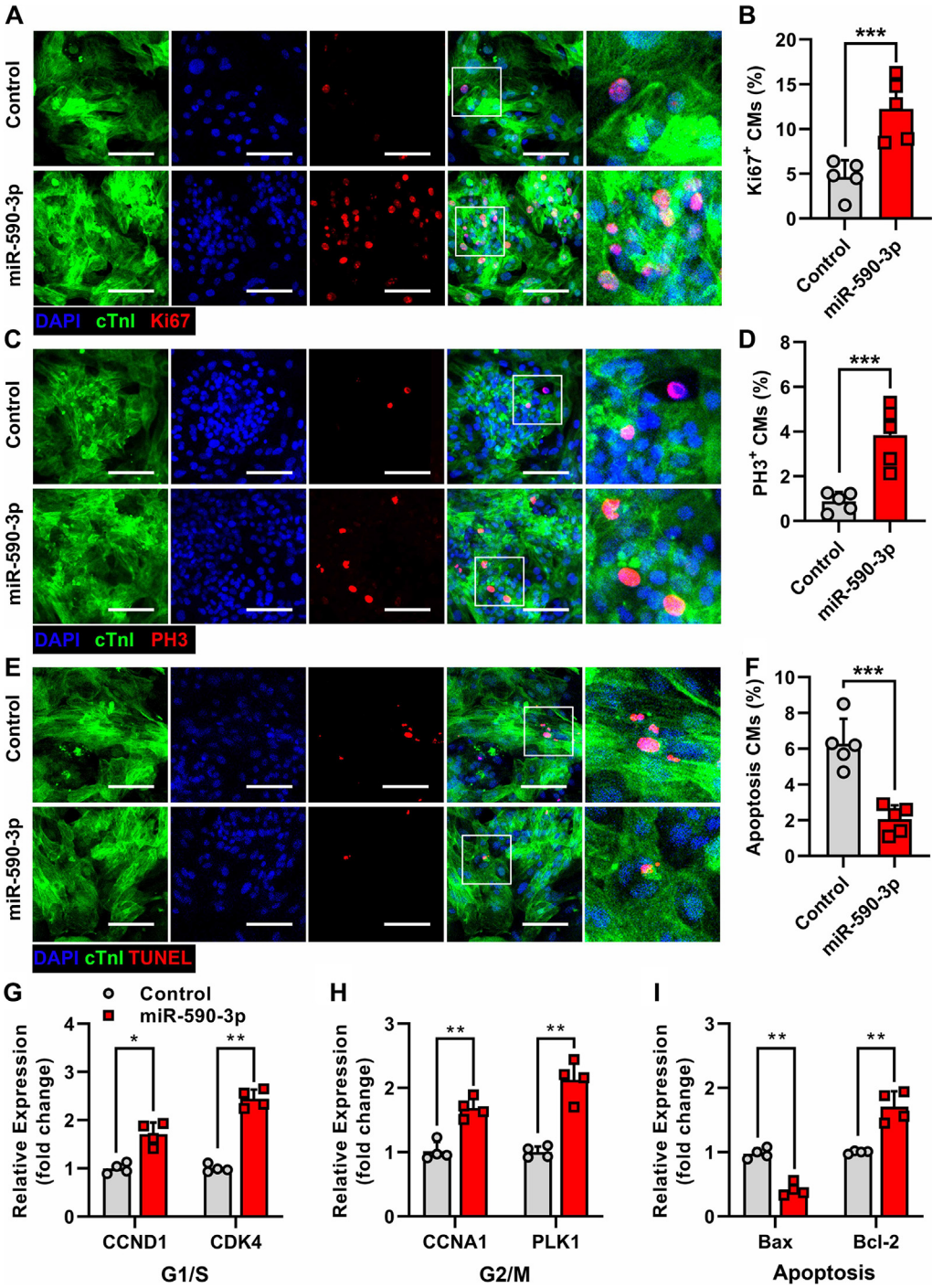

(A) Representative images of hiPSC-CMs positive for the proliferation marker Ki67. (B) Number of Ki67-positive cells in control and miR-590-3p-overexpressing hiPSC-CMs (n = 5; 5 random fields per sample). (C) Representative images of hiPSC-CMs positive for the M-phase marker PH3. (D) Number of PH3-positive cells in control and miR-590-3p-OE hiPSC-CMs (n = 5; 5 random fields per sample). (E) Representative images of apoptotic (TUNEL-positive) hiPSC-CMs. (F) Number of TUNEL-positive control and miR-590-3p-OE hiPSC-CMs (n = 5; 5 random fields per sample). (G to I) Relative expression levels of (G and H) cell cycle and (I) apoptosis genes in control and miR-590-3p-OE hiPSC-CMs (n = 4). Scale bar: 50 μm. Data are presented as mean ± SD. *P* values were determined using the unpaired Student's *t*-test. **P* < 0.05, ***P* < 0.01, and ****P* < 0.001. Bcl-2 = B-cell lymphoma-2; Bax = Bcl-2 associated X; CM = cardiomyocyte; hiPSC-CM = human induced pluripotent stem cell-derived cardiomyocyte; miR = microRNA; TUNEL = transferase-mediated deoxyuridinetriphate nick-end labeling.

ability of hiPSC-CMs to improve cardiac function and reduce fibrosis after MI.

miR-590-3p OVEREXPRESSION INCREASED THE NUMBER OF ENGRAFTED hiPSC-CMs, PROMOTED ANGIOGENESIS, AND INHIBITED CARDIOMYOCYTE HYPERTROPHY IN INFARCTED MOUSE HEARTS. BLI and immunofluorescence staining were performed to investigate whether miR-590-3p overexpression increased the number of engrafted hiPSC-CMs after cell transplantation (**Figure 5A**). Luciferase-hiPSC-CMs (5.0×10^5 cells) were injected into the infarcted myocardium. BLI analysis showed that the luciferin signal was higher in animals receiving miR-590-3p-OE hiPSC-CMs than in controls at day 28 after cell delivery (**Figures 5B and 5C**). In line with this observation, immunofluorescence staining showed that the area occupied by transplanted hiPSC-CMs (stained with human-specific cardiac troponin T [green fluorescence]) was significantly greater in mice receiving miR-590-3p-OE hiPSC-CMs than in controls at day 28 after cell delivery (**Figures 5D and 5E**). qRT-PCR results demonstrated that the expression of the *SRY* gene (transplanted cells indicator) demonstrated that there were more miR-590-3p-OE hiPSC-CMs in the heart than in controls after transplantation (Supplemental Figure 3). The results showed that miR-590-3p promoted the proliferation and expansion of the graft in vivo.

The ability of miR-590-3p to induce cellular proliferation was assessed by measuring the number of transplanted hiPSC-CMs expressing the proliferation markers Ki67 and PH3 via immunofluorescence staining. The expression levels of Ki67 and PH3 were 2- and 4-fold higher, respectively, in miR-590-3p-OE cells than in control cells (**Figures 6A to 6D**). qRT-PCR analysis indicated that the expression levels of the proliferation-related genes *CCNB1*, *CCND1*, *CDK4*, and *PLK1* were remarkably higher in myocardium treated with miR-590-3p-OE hiPSC-CMs than in hearts treated with control cells (Supplemental Figures 4A to 4D). We also assessed whether miR-590-3p-OE hiPSC-CMs could induce the proliferation of endogenous cardiomyocytes. The proportion of Ki67-positive endogenous cardiomyocytes was significantly higher in the infarct border zone of animals treated with miR-590-3p-OE hiPSC-CMs (**Figures 6E and 6F**).

Angiogenesis plays a critical role in myocardial repair following MI. Therefore, we measured microvessel density by CD31 immunofluorescence staining in the infarct border zone at day 28 post-MI. The results showed that microvessel density was almost 2-fold higher in the infarct border zone of animals treated with miR-590-3p-OE hiPSC-CMs than in the myocardium of animals treated with control cells (**Figures 7A and 7B**).

The protective function of hiPSC-CMs on cardiac hypertrophy was assessed by measuring the cross-sectional surface area of native cardiomyocytes in the infarct border zone. The cross-sectional surface area of cardiomyocytes was significantly smaller in the infarct border zone of animals treated with miR-590-3p-OE hiPSC-CMs than in animals treated with control cells (**Figures 7C and 7D**). These results indicated that miR-590-3p overexpression increased the ability of hiPSC-CMs to promote angiogenesis and inhibit cardiomyocyte hypertrophy.

miR-590-3p-OE hiPSC-CM TREATMENT IMPROVED CARDIAC FUNCTION BY STIMULATING hiPSC-CM PROLIFERATION IN A PIG MODEL OF MI. We evaluated the ability of miR-590-3p-OE hiPSC-CMs to repair MI. The experimental workflow is illustrated in **Figure 8A**. Cardiac function was evaluated 28 days after MI by high-resolution computed tomography. Both control hiPSC-CMs and miR-590-3p-OE hiPSC-CMs enhanced left ventricular ejection fraction and left ventricular fractional shortening while reducing LVEDV and LVESV. In addition, cardiac function was better in the miR-590-3p-OE hiPSC-CM group than in the control group (**Figures 8B to 8E**). Similarly, the analyses of fresh heart slides showed that hiPSC-CM transplantation reduced scar size, and miR-590-3p-OE hiPSC-CMs had a stronger effect on scar reduction. Thus, miR-590-3p-OE hiPSC-CM transplantation has therapeutic potential for MI.

Analysis of Ki67 and PH3 expression by immunofluorescence staining showed that miR-590-3p significantly enhanced hiPSC-CM proliferation in porcine hearts. (Supplemental Figures 5A to 5D). We next assessed the safety of using miR-590-3p-OE hiPSC-CMs in pig hearts. Blood cell analysis showed that the number of monocytes increased slightly after hiPSC-CM delivery, and this increase might be caused by the surgical procedure (Supplemental Figures 6A to 6D). The levels of serum chemistry in hepatic, renal, and cardiac analyses did not change significantly after hiPSC-CM transplantation in the control and miR-590-3p groups (Supplemental Figures 6E to 6H). In addition, continuous electrocardiogram recordings detected by a telemetry device showed that miR-590-3p-OE hiPSC-CM transplantation did not cause an increase in arrhythmic events (premature ventricular contractions and nonsustained ventricular tachycardia) (Supplemental Figures 6I and 6J). These results demonstrated the safety and efficacy of the transplantation of miR-590-3p-OE hiPSC-CMs.

FIGURE 3 miR-590-3p Promotes the Proliferation of hiPSC-CMs by Regulating the TSC22D2/Pkm2 Pathway

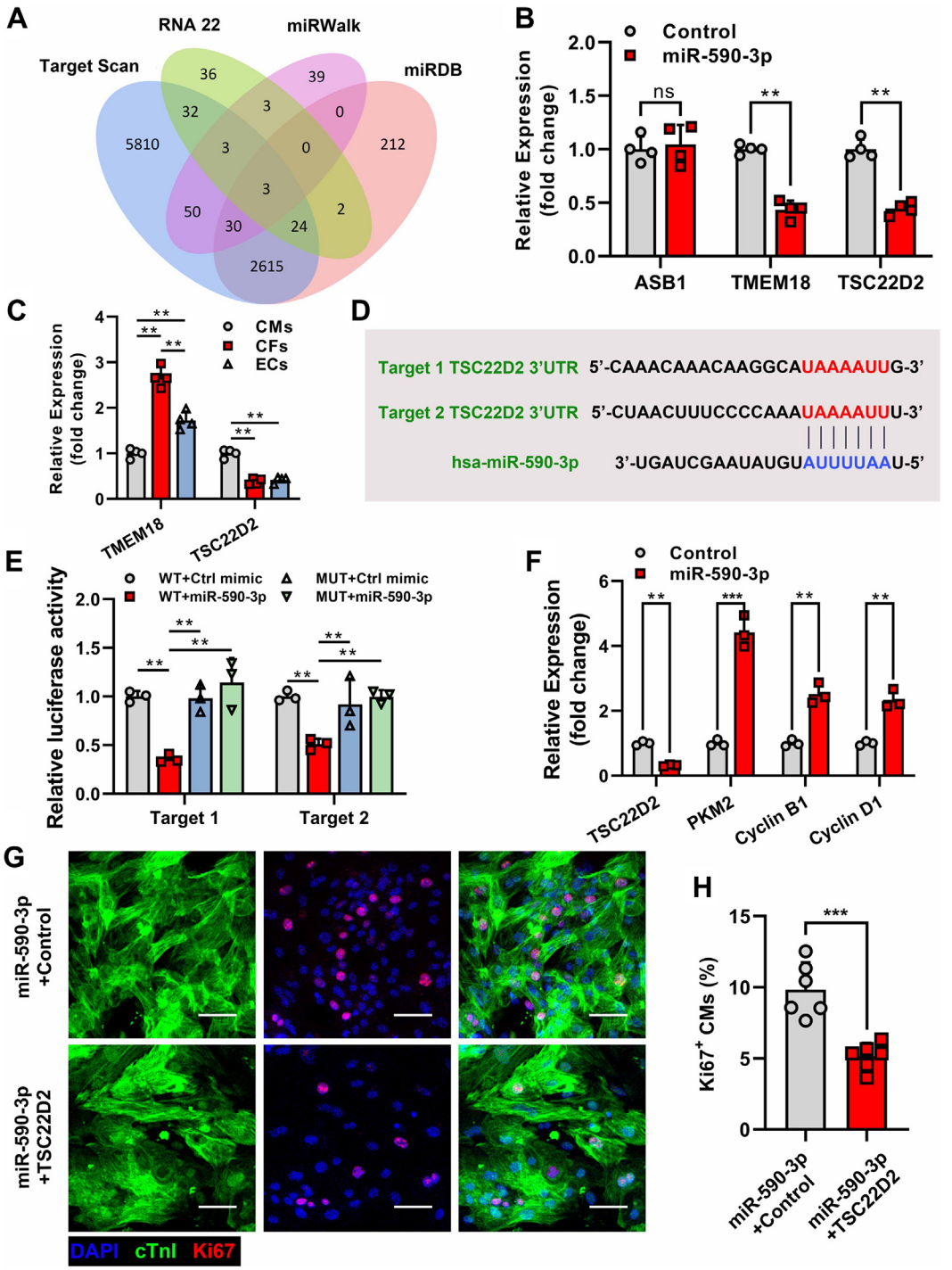

(A) Venn diagram of miR-590-3p potential target genes. (B) Analysis of the relative expression levels of *ASB1*, *TMEM18*, and *TSC22D2* in hiPSC-CMs by qRT-PCR after miR-590-3p treatment (n = 4). (C) Relative expression levels of *TMEM18* and *TSC22D2* in CMs, CFs, and ECs (n = 4). (D) Potential binding sites for miR-590-3p in the 3′-UTR of *TSC22D2*. (E) Luciferase reporter activity of chimeric vectors carrying the luciferase gene and a fragment of *TSC22D2* containing WT or mutation binding sites for miR-590-3p. (F) Western blot analysis of the protein expression of TSC22D2, PKM2, cyclin B1, and cyclin D1 (n = 3). (G) Representative images of hiPSC-CMs positive for the proliferation marker Ki67. (H) Number of Ki67-positive cells (n = 5; 5 random fields per sample). Scale bar: 50 μm. Data are presented as mean ± SD. *P* values were determined using the unpaired Student's *t*-test or 1-way analysis of variance followed by Tukey's post hoc test. $^{**}P < 0.01$ and $^{***}P < 0.001$. ASB1 = ankyrin repeat and SOCS box containing 1; CF = cardiac fibroblast; cTnI = cardiac troponin I; Ctrl = control; DAPI = 4',6-diamidino-2-phenylindole; EC = endothelial cell; MUT = mutation; ns = not significant; PKM2 = pyruvate kinase M2; TMEM18 = transmembrane protein 18; TSC22D2 = TSC22 domain family member 2; UTR = untranslated region; WT = wild type; other abbreviations as in Figure 1 and 2.

FIGURE 4 **miR-590-3p Overexpression Improves the Therapeutic Effect of hiPSC-CM Transplantation on Cardiac Repair After MI**

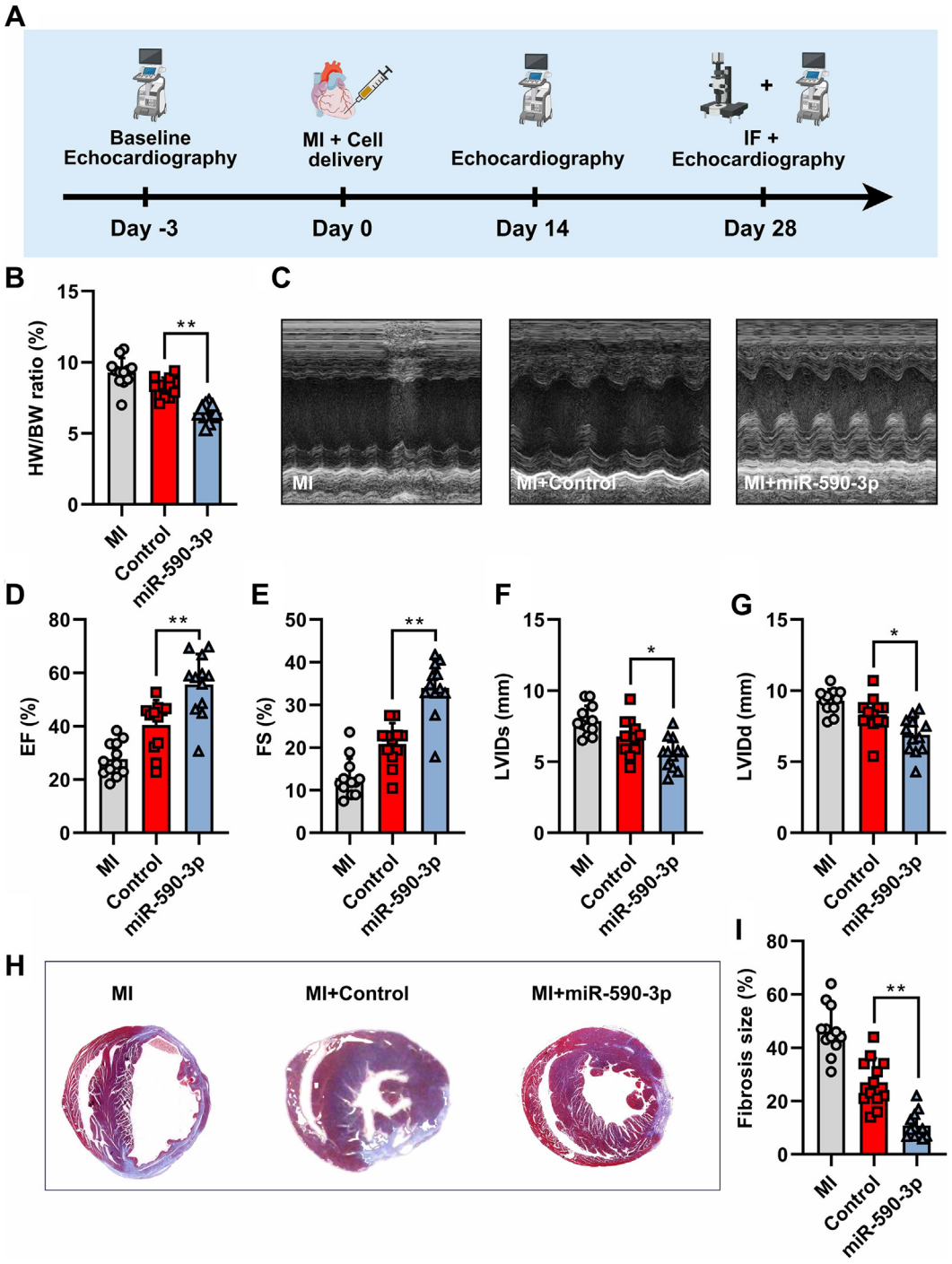

(A) Timeline of mouse MI in vivo. (B) Quantification of the HW/BW ratio (n = 12). (C) Representative echocardiographic images. (D to G) Echocardiographic assessment of EF%, FS%, LVIDs, and LVIDd (n = 12). (H) Fibrotic area in infarcted mouse hearts. (I) Quantification of fibrosis (n = 12). Data are presented as mean ± SD. *P* values were determined using 1-way analysis of variance followed by Tukey's post hoc test. *$P < 0.05$ and **$P < 0.01$. BW = body weight; EF = ejection fraction; FS = shortening fraction; HW = heart weight; LVIDd = left ventricular internal diameter at end diastole; LVIDs = left ventricular internal diameter at end systole; MI = myocardial infarction; other abbreviations as in Figures 1 and 2.

FIGURE 5 **miR-590-3p Overexpression Increases the Engraftment Rates of hiPSC-CMs in Infarcted Mouse Hearts After Cell Transplantation**

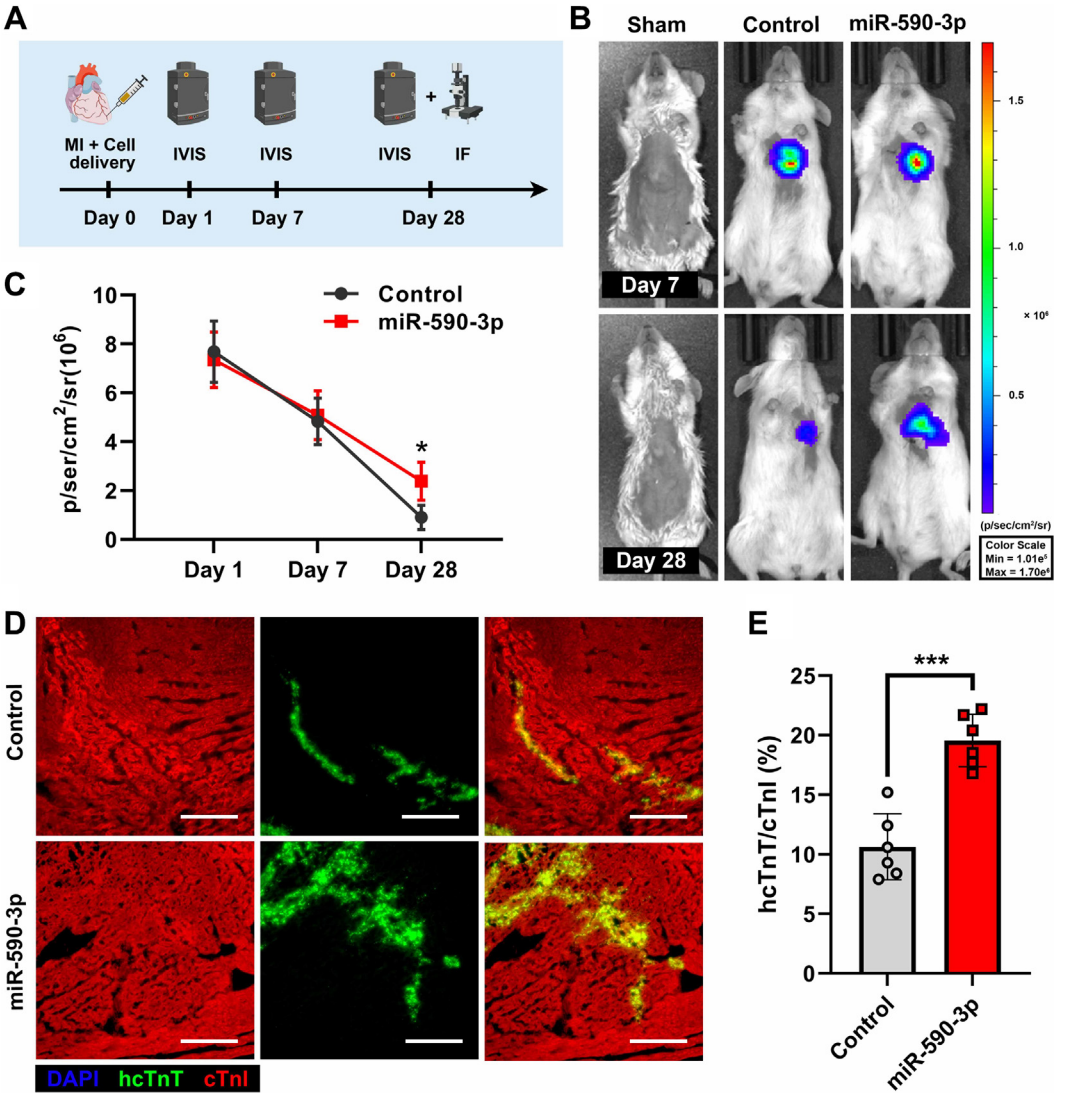

(A) Timeline of the in vivo study. (B) Representative BLI images of hearts implanted with miR-590-3p-overexpressing hiPSC-CMs or control cells. (C) Quantification of BLI fluorescence intensity (n = 6). (D) IF staining of hiPSC-CMs in infarcted hearts. (E) Quantification of the engraftment rates of hiPSC-CMs in infarcted hearts (n = 6). Scale bar = 200 μm. Data are presented as mean ± SD. *P* values were determined using unpaired Student's *t*-test. *$P < 0.05$ and ***$P < 0.001$. BLI = bioluminescence live imaging; hcTnT = human cardiac troponin T; IVIS = image visualization and infrared spectroscopy; Max = maximum; Min = minimum; other abbreviations as in Figures 1 to 4.

DISCUSSION

Severe MI usually results in a significant loss of cardiomyocytes. During the early stage of MI, cardiac fibroblasts are activated and produce extracellular matrix (ECM) in response to new hemodynamic conditions.[17] However, the loss of cardiomyocytes and excessive ECM deposition causes changes in cardiac structure, impairing function and ultimately leading to HF. hiPSC-CM transplantation is a potentially effective therapeutic strategy for heart tissue repair. However, several critical issues need to be resolved before clinical application. Our results demonstrated that miR-590-3p enhanced the ability of hiPSC-CMs to improve MI by regulating the TSC22D2/PKM2 pathway.

Low engraftment rates after cell transplantation are one of the primary obstacles to achieving the

FIGURE 6 miR-590-3p Overexpression Promotes the Proliferation of hiPSC-CMs in Infarcted Mouse Hearts After Cell Transplantation

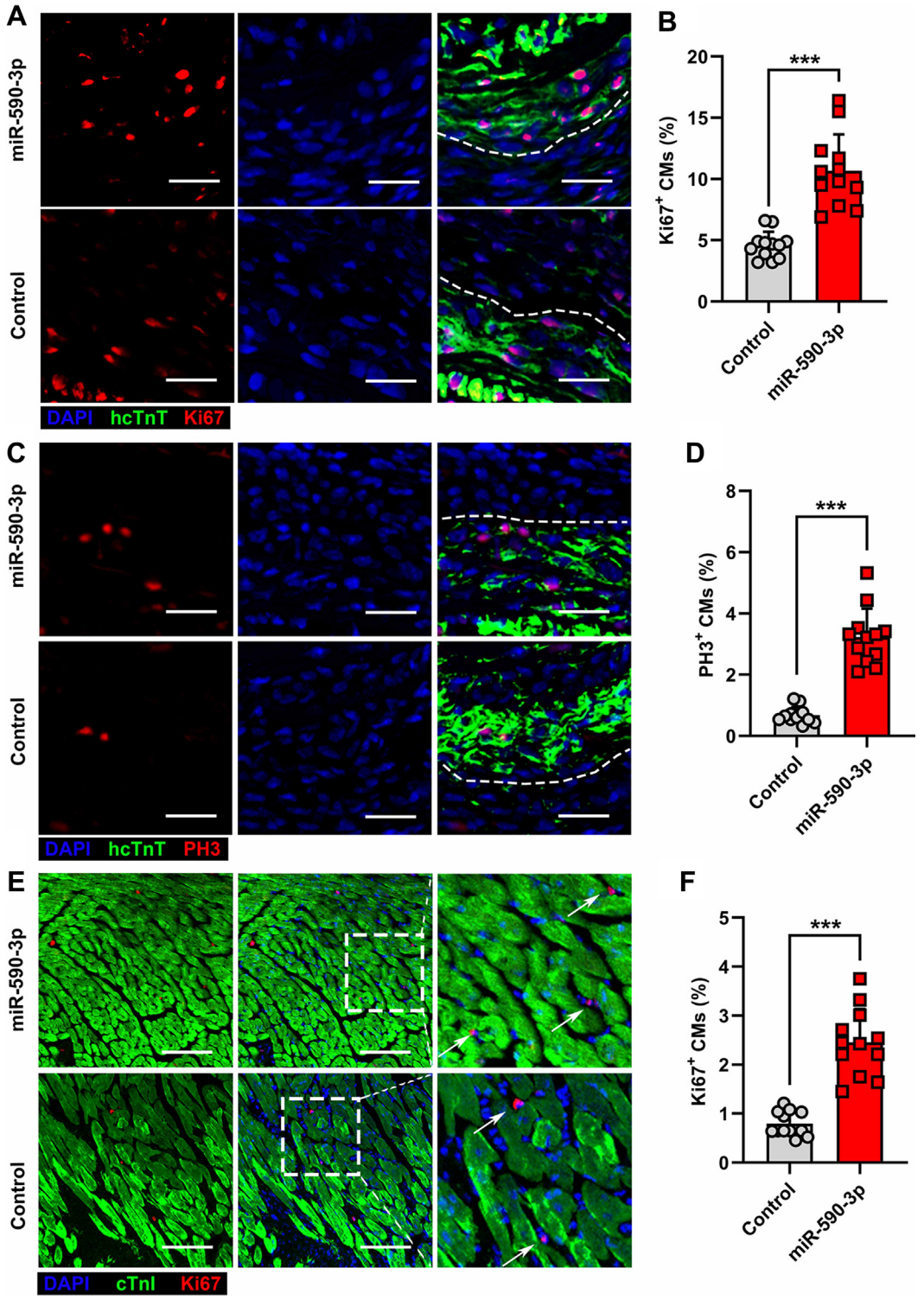

(A) Representative images of implanted hiPSC-CMs positive for the proliferation marker Ki67. (B) Number of Ki67-positive control and miR-590-3p–overexpressing (OE) hiPSC-CMs (n = 12; 5 random fields per sample). (C) Representative images of implanted hiPSC-CMs positive for the M-phase marker PH3. (D) Number of PH3-positive control and miR-590-3p-OE hiPSC-CMs (n = 12; 5 random fields per sample). (E) Treatment with miR-590-3p-OE hiPSC-CMs induces the proliferation of endogenous cardiomyocytes. Representative images of Ki67-positive endogenous cardiomyocytes in the infarct border zone. (F) Number of Ki67-positive endogenous cardiomyocytes (n = 12; 5 random fields per sample). Data are presented as mean ± SD. *P* values were determined using the unpaired Student's *t*-test. ***$P < 0.001$. Abbreviations as in Figures 1 to 3.

FIGURE 7 Treatment With miR-590-3p-Overexpressing hiPSC-CMs Promotes Angiogenesis and Inhibits Cardiomyocyte Hypertrophy in a Mouse Model of Myocardial Infarction

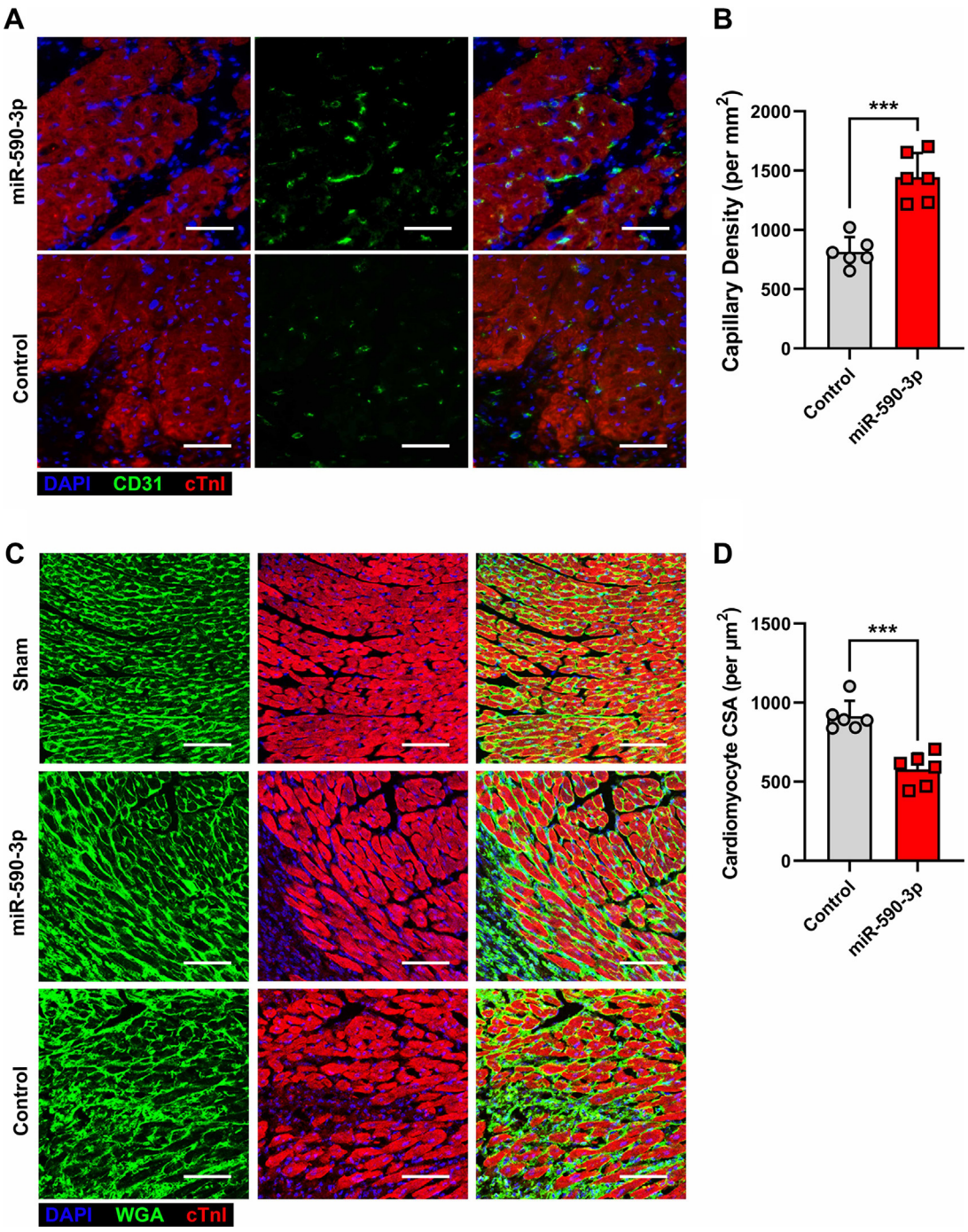

(A) Representative images of microvessels immunostained with troponin I (red) and CD31 (green). Scale bar: 50 μm. (B) Quantification of microvessel density by calculating the number of CD31-positive cells per mm^2 (n = 6, 5 random fields per sample). (C) Representative images of cardiomyocytes immunostained with WGA-FITC (red) and troponin I (green) in the infarct border zone. Scale bar: 100 μm. (D) Quantification of the CSA of cardiomyocytes by WGA-FITC staining (n = 6, 5 random fields per sample). Data are presented as mean ± SD. P-values were determined using unpaired Student's *t*-test. *** $P < 0.001$. CSA = cross-sectional area; FITC = fluorescein isothiocyanate; WGA = wheat germ agglutinin; other abbreviations as in Figures 1 and 4.

FIGURE 8 miR-590-3p–Overexpressing hiPSC-CMs Ameliorates Myocardial Function and Mitigates Cardiac Infarct Size in a Porcine MI Model

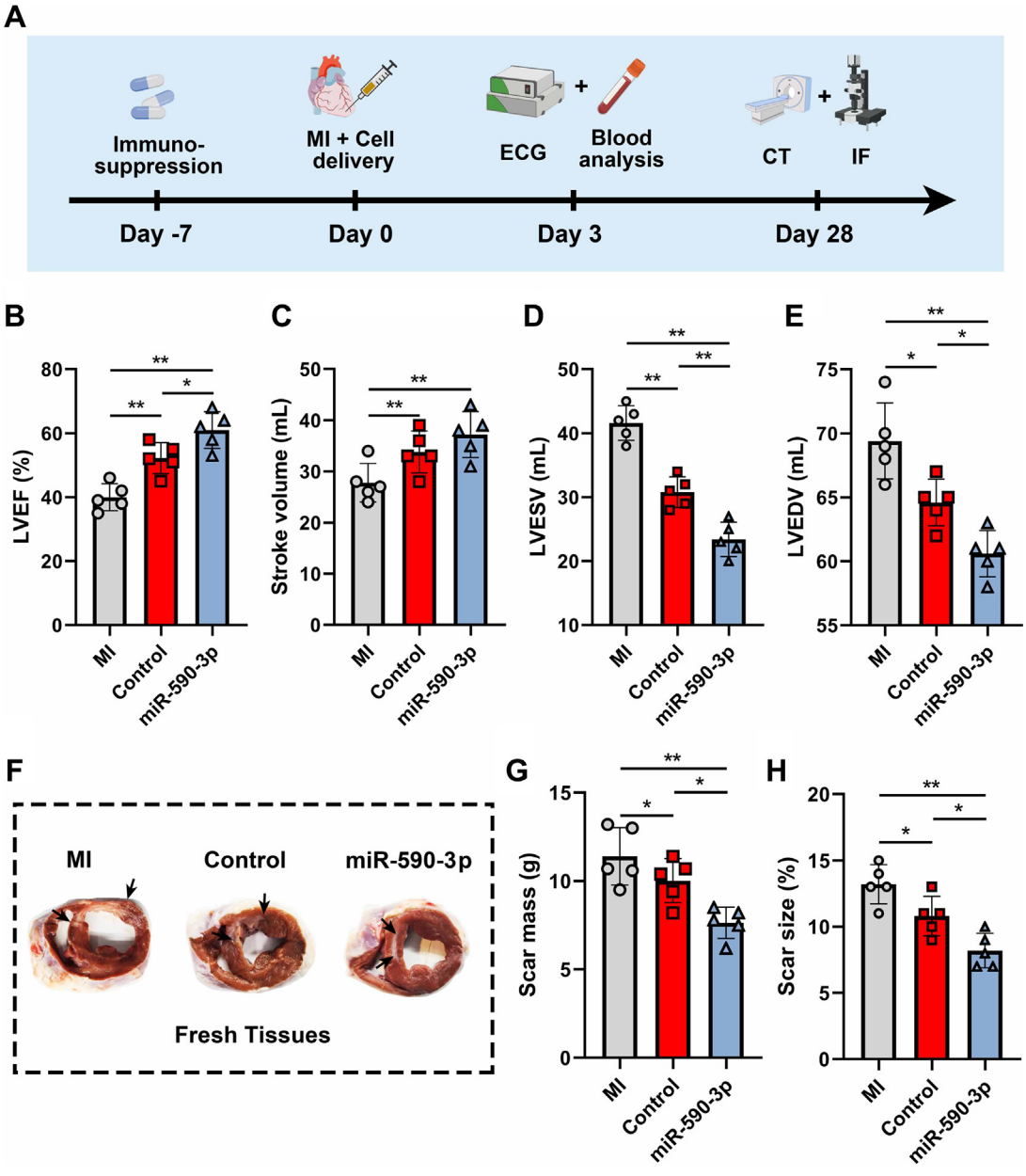

(A) Experimental procedures. (B to E) Quantification of (B) LVEF, (C) stroke volume, (D) LVEDV, and (E) LVESV assessed by CT. (F) Representative images of fresh cardiac tissues of scar mass and size analysis on day 28 after MI. (G and H) Quantification of scar mass and size. n = 5 animals per group. Data are presented as mean ± SD. *P* values were determined using 1-way analysis of variance followed by Tukey's post hoc test. *$P < 0.05$ and **$P < 0.01$. CT = computed tomography; ECG = electrocardiogram; IF = immunofluorescence; LVEF = left ventricular ejection fraction; LVEDV = left ventricular end-diastolic volume; LVESV = left ventricular end-systolic volume; MI = myocardial infarction; miR = microRNA.

functional regeneration of injured hearts through stem cell therapy.[18,19] This study provides the first evidence that miR-590-3p stimulates the proliferation of hiPSC-CMs in vivo and in vitro. Moreover, miR-590-3p increased the hiPSC-CM engraftment rate, improving cardiac function and reducing cardiac fibrosis and hypertrophy after MI.

In mammalian fetuses, approximately 3% to 15% of cardiomyocytes are in the cell cycle,[20] which increases cardiac regeneration capacity by stimulating cardiomyocyte division. Gene expression profiling and proteomics analysis identified several factors that increase the proliferative capacity of cardiomyocytes, and in vivo studies demonstrated that proliferative genes stimulated mitosis in adult mammalian cardiomyocytes after MI.[21] Similar to adult cardiomyocytes, the proliferative capacity of hiPSC-CMs decreases with prolonged culturing, and hiPSC-CMs initiate maturation and exit the cell cycle after transplantation.[22] Our results demonstrated the ability of miR-590-3p to promote cellular proliferation. We found that the expression of miR-590-3p decreased during cardiac maturation. Gain-of-function experiments demonstrated that miR-590-3p promoted hiPSC-CM proliferation. miR-590-3p also increased the number of proliferating hiPSC-CMs in vitro by more than 2-fold and increased the engraftment rate of implanted hiPSC-CMs by more than 1.5-fold in a mouse model of MI. Furthermore, the expression of proliferation markers Ki67 and PH3 was significantly up-regulated in cardiomyocytes receiving miR-590-3p-OE hiPSC-CMs, suggesting that paracrine factors secreted by hiPSC-CMs induce endogenous cardiomyocyte proliferation.

The effect of miR-590-3p on cell proliferation varies depending on the disease model and cell type. For instance, Salem et al[23] demonstrated that miR-590-3p promoted ovarian cancer growth and metastasis by enhancing tumor cell proliferation.[23] Conversely, Wang et al[24] observed that miR-590-3p inhibited osteosarcoma cell proliferation and metastasis by regulating SRY-box transcription factor 9 (SOX9).[24] The varying effect of miR-590-3p on tumor cell proliferation in different cancers may be related to the target genes it regulates and the expression of target genes in tumor cells. miR-590-3p promotes endogenous cardiomyocyte proliferation in rodents. However, little is known about the function of miR-590-3p in hiPSC-CM proliferation. Our results showed that miR-590-3p increased hiPSC-CM proliferation, whereas other studies found that miR-590-3p promoted hiPSC-CM proliferation to a small extent. This discrepancy may be attributable to the different iPSC cell lines used across studies and differences in gene expression and biological functions among cell lines. Therefore, a comprehensive assessment of the role of miR-590-3p in iPSC cell lines can help develop hiPSC-CM–based therapeutic strategies for MI.

Uncontrolled cardiomyocyte proliferation increases the risk of death in patients with MI. Gabisonia et al[6] reported that the expression of human miRNA-199a in infarcted pig hearts stimulated cardiac repair. However, the persistent and uncontrolled expression of this miRNA resulted in the sudden arrhythmic death of treated pigs. These results indicate that achieving cardiac repair by stimulating endogenous cardiomyocyte proliferation is attainable in large mammals; however, the dosage of this therapy needs to be tightly controlled. In our study, 5.0×10^7 cells were transplanted into infarcted hearts.[19] Previous studies reported that mechanical action and electrical activity promoted hiPSC-CM maturation. Moreover, graft cells matured 30 days after hiPSC-CM transplantation in neonatal mice.[25] These results confirm that the proliferative capacity of hiPSC-CMs decreases after transplantation while their contractile and metabolic functions increase. Furthermore, our experimental results confirmed that miR-590-3p-OE hiPSC-CM transplantation was not associated with an increase in arrhythmic events, demonstrating that miR-590-3p-OE hiPSC-CM transplantation is safe and effective for treating MI.

Cardiac fibrosis causes ventricular systolic dysfunction. In addition, cardiac overload and nutrient deficiency contribute to cardiomyocyte hypertrophy in the peri-infarct zone. Therefore, even after recovering from initial infarction, fibrosis affects the viability of peri-infarct zone cardiomyocytes through the disintegration of the ECM and replacement of necrotic tissue by scar tissue.[26] We found that hiPSC-CM transplantation restored cardiac function, increased microvessel density, and reduced cardiomyocyte hypertrophy and that miR-590-3p overexpression enhanced these effects.

Because of differences in hemodynamic and electrophysiologic properties between mice and humans, research data from rodent models cannot be translated to humans.[27] Nonetheless, preclinical animal models, such as pigs and nonhuman primates, are essential to assess clinical safety. Gabisonia et al[6] reported that intramyocardial injections of miR-199a induced endogenous cardiomyocyte proliferation, improving functional recovery in a pig model of MI. However, uncontrolled endogenous cardiomyocyte proliferation mediated by miR-199 overexpression predisposed to ventricular arrhythmias, leading to sudden death.[6] Our study assessed the safety of using miR-590-3p-OE hiPSC-CMs in pig hearts. The number

of blood cells; the levels of inflammatory cytokines in the pericardial fluid; and the levels of hepatic, renal, and cardiac markers have no difference between miR-590-3p-OE hiPSC-CM and control hiPSC-CM administration.

STUDY LIMITATIONS. In the present study, we analyzed the phenotype of the mouse/pig model 4 weeks after MI. Although miR-590-3p-OE hiPSC-CMs showed a restorative effect on cardiac function in the early stages of MI, further research is required to assess myocardial recovery in the long run.

CONCLUSIONS

The results showed that miR-590-3p overexpression promoted hiPSC-CM proliferation in vitro and in vivo. Further, miR-590-3p improved the therapeutic effect of hiPSC-CMs on MI by increasing the engraftment rate. Importantly, we confirmed the safety of using miR-590-3p-OE hiPSC-CMs in pig hearts. These results demonstrate that the transplantation of miR-590-3p-OE hiPSC-CMs is potentially effective for cardiac regeneration.

FUNDING SUPPORT AND AUTHOR DISCLOSURES

This work was supported by the National Key Research and Development Program of China (2020YFA0112600), the National Natural Science Foundation of China (No. 81970397), and the Preresearch Fund Project of the Second Affiliated Hospital of Soochow University (SDFEYQN1914). The authors have reported that they have no relationships relevant to the contents of this paper to disclose.

ADDRESSES FOR CORRESPONDENCE: Dr Ling Gao, Translational Medical Center for Stem Cell Therapy & Institute for Regenerative Medicine, Shanghai East Hospital, Tongji University School of Medicine, 1800 Yuntai Road, Shanghai 200123, China. E-mail: gaoleng5@126.com. OR Dr Qingyou Meng, Department of Vascular Surgery, General Surgery Clinical Center, Shanghai General Hospital, Shanghai Jiao Tong University School of Medicine, 100 Haining Road, Shanghai 200080, China. E-mail: mengqy@163.com.

PERSPECTIVES

COMPETENCY IN MEDICAL KNOWLEDGE: We have demonstrated that miR-590-3p–overexpressed hiPSC-CMs enhance cardiac function 28 days after MI in a preclinical pig model. With potential clinical trials in the near future, the safety of the treatment was also evaluated in this paper. We found that the transplantation of miR-590-3p–overexpressed hiPSC-CMs is potentially effective for cardiac regeneration.

TRANSLATIONAL OUTLOOK: miR-590-3p improved the therapeutic effect of hiPSC-CMs on MI by increasing the engraftment rate. This may present potential new strategies for treating MI, thus helping the development of novel therapeutics.

REFERENCES

1. Pfeffer MA, Shah AM, Borlaug BA. Heart failure with preserved ejection fraction in perspective. *Circ Res*. 2019;124:1598–1617.

2. Mahmoud AI, Kocabas F, Muralidhar SA, et al. Meis1 regulates postnatal cardiomyocyte cell cycle arrest. *Nature*. 2013;497:249–253.

3. Ichihara Y, Kaneko M, Yamahara K, et al. Self-assembling peptide hydrogel enables instant epicardial coating of the heart with mesenchymal stromal cells for the treatment of heart failure. *Biomaterials*. 2018;154:12-23.

4. Jung JH, Ikeda G, Tada Y, et al. miR-106a-363 cluster in extracellular vesicles promotes endogenous myocardial repair via Notch3 pathway in ischemic heart injury. *Basic Res Cardiol*. 2021;116:19.

5. Qian L, Huang Y, Spencer CI, et al. In vivo reprogramming of murine cardiac fibroblasts into induced cardiomyocytes. *Nature*. 2012;485:593–598.

6. Gabisonia K, Prosdocimo G, Aquaro GD, et al. MicroRNA therapy stimulates uncontrolled cardiac repair after myocardial infarction in pigs. *Nature*. 2019;569:418–422.

7. Kolanowski TJ, Busek M, Schubert M, et al. Enhanced structural maturation of human induced pluripotent stem cell-derived cardiomyocytes under a controlled microenvironment in a microfluidic system. *Acta Biomater*. 2020;102:273–286.

8. Ebert A, Joshi AU, Andorf S, et al. Proteasome-dependent regulation of distinct metabolic states during long-term culture of human iPSC-derived cardiomyocytes. *Circ Res*. 2019;125:90–103.

9. Shiba Y, Gomibuchi T, Seto T, et al. Allogeneic transplantation of iPS cell-derived cardiomyocytes regenerates primate hearts. *Nature*. 2016;538:388–391.

10. Lu TX, Rothenberg ME. MicroRNA. *J Allergy Clin Immunol*. 2018;141:1202–1207.

11. Du WW, Yang W, Xuan J, et al. Reciprocal regulation of miRNAs and piRNAs in embryonic development. *Cell Death Differ*. 2016;23:1458–1470.

12. Eulalio A, Mano M, Dal Ferro M, et al. Functional screening identifies miRNAs inducing cardiac regeneration. *Nature*. 2012;492:376–381.

13. Gao F, Kataoka M, Liu N, et al. Therapeutic role of miR-19a/19b in cardiac regeneration and protection from myocardial infarction. *Nat Commun*. 2019;10(1):1802.

14. Lesizza P, Prosdocimo G, Martinelli V, Sinagra G, Zacchigna S, Giacca M. Single-dose intracardiac injection of pro-regenerative microRNAs improves cardiac function after myocardial infarction. *Circ Res*. 2017;120:1298–1304.

15. Gao L, Wang L, Wei Y, et al. Exosomes secreted by hiPSC-derived cardiac cells improve recovery from myocardial infarction in swine. *Sci Transl Med*. 2020;12(561):eaay1318.

16. Liang F, Li Q, Li X, et al. TSC22D2 interacts with PKM2 and inhibits cell growth in colorectal cancer. *Int J Oncol*. 2016;49:1046–1056.

17. Li L, Zhao Q, Kong W. Extracellular matrix remodeling and cardiac fibrosis. *Matrix Biol*. 2018;68-69:490–506.

18. Zhao M, Fan C, Ernst PJ, et al. Y-27632 preconditioning enhances transplantation of human-induced pluripotent stem cell-derived cardiomyocytes in myocardial infarction mice. *Cardiovasc Res*. 2019;115:343–356.

19. Zhao M, Nakada Y, Wei Y, et al. Cyclin D2 overexpression enhances the efficacy of human induced pluripotent stem cell-derived

cardiomyocytes for myocardial repair in a swine model of myocardial infarction. *Circulation*. 2021;144:210–228.

20. Zhao M, Zhang E, Wei Y, Zhou Y, Walcott GP, Zhang J. Apical resection prolongs the cell cycle activity and promotes myocardial regeneration after left ventricular injury in neonatal pig. *Circulation*. 2020;142:913–916.

21. Magadum A, Singh N, Kurian AA, et al. Pkm2 regulates cardiomyocyte cell cycle and promotes cardiac regeneration. *Circulation*. 2020;141:1249–1265.

22. Feyen DAM, McKeithan WL, Bruyneel AAN, et al. Metabolic maturation media improve physiological function of human iPSC-derived cardiomyocytes. *Cell Rep*. 2020;32:107925.

23. Salem M, O'Brien JA, Bernaudo S, et al. miR-590-3p promotes ovarian cancer growth and metastasis via a novel FOXA2-versican pathway. *Cancer Res*. 2018;78:4175–4190.

24. Wang WT, Qi Q, Zhao P, Li CY, Yin XY, Yan RB. miR-590-3p is a novel microRNA which suppresses osteosarcoma progression by targeting SOX9. *Biomed Pharmacother*. 2018;107:1763–1769.

25. Kadota S, Pabon L, Reinecke H, Murry CE. In vivo maturation of human induced pluripotent stem cell-derived cardiomyocytes in neonatal and adult rat hearts. *Stem Cell Rep*. 2017;8:278–289.

26. Kim GH, Uriel N, Burkhoff D. Reverse remodelling and myocardial recovery in heart failure. *Nat Rev Cardiol*. 2018;15:83–96.

27. Liu S, Li K, Wagner Florencio L, et al. Gene therapy knockdown of Hippo signaling induces cardiomyocyte renewal in pigs after myocardial infarction. *Sci Transl Med*. 2021;13(600):eabd6892.

KEY WORDS cell cycle, human induced pluripotent stem cells, miR-590-3p, myocardial infarction

APPENDIX For supplemental tables and figures, please see the online version of this paper.